

Coupled-channels analysis of the $^{16}\text{O}+^{208}\text{Pb}$ fusion barrier distribution

C.R. Morton, A.C. Berriman, M. Dasgupta, D.J. Hinde, and J.O. Newton
*Department of Nuclear Physics, Research School of Physical Sciences and Engineering,
Australian National University, Canberra, ACT 0200, Australia*

K. Hagino

*Institute for Nuclear Theory, Department of Physics, University of Washington, Seattle, WA
98195-1550*

I.J. Thompson

Physics Department, University of Surrey, Guildford GU2 5XH, United Kingdom

(Received 28 April 1999, Accepted for publication in Phys. Rev. **C**)

Abstract

Analyses using simplified coupled-channels models have been unable to describe the shape of the previously measured fusion barrier distribution for the doubly magic $^{16}\text{O}+^{208}\text{Pb}$ system. This problem was investigated by re-measuring the fission excitation function for $^{16}\text{O}+^{208}\text{Pb}$ with improved accuracy and performing more exact coupled-channels calculations, avoiding the constant-coupling and first-order coupling approximations often used in simplified analyses. Couplings to the single- and 2-phonon states of ^{208}Pb , correctly taking into account the excitation energy and the phonon character of these states, particle transfers, and the effects of varying the diffuseness of the nuclear potential, were all explored. However, in contrast to other recent analyses of precise fusion data, no satisfactory simultaneous description of the

shape of the experimental barrier distribution and the fusion cross-sections
for $^{16}\text{O}+^{208}\text{Pb}$ was obtained.

PACS number: 25.70.Jj, 24.10.Eq, 21.60.Ev, 27.80.+w

I. INTRODUCTION

Precise fusion cross-sections have been measured for many reactions, involving nuclei which exhibit different collective degrees of freedom. Their excitations, through coupling to the relative motion of the colliding nuclei, cause a splitting in energy of the single fusion barrier resulting in a distribution of barriers, which drastically alters the fusion probability from its value calculated assuming quantal tunnelling through a single barrier. It was shown by Rowley *et al.* [1] that, under certain approximations, the distribution in energy of a discrete spectrum of barriers could be obtained from precise fusion cross-sections σ by taking the second derivative with respect to the center-of-mass energy $E_{c.m.}$ of the quantity $(E_{c.m.}\sigma)$. When the effects of quantal tunnelling are considered, $d^2(E_{c.m.}\sigma)/dE_{c.m.}^2$ becomes continuous, and each barrier is smoothed in energy with a full width at half maximum (FWHM) of $0.56\hbar\omega$, where $\hbar\omega$ is the barrier curvature. The difference between a more realistic calculation of $d^2(E_{c.m.}\sigma)/dE_{c.m.}^2$ (where the angular momentum dependence of the curvature and barrier radius is taken into account) and the smoothed barrier distribution is small [2], and so it is convenient to refer to $d^2(E_{c.m.}\sigma)/dE_{c.m.}^2$ as the fusion barrier distribution.

The fusion barrier distribution can be a very sensitive ‘gauge’ of the dominant collective modes excited during the collision [2]. Its shape is related to the nuclear structure of the reactants. Barrier distributions have been measured for nuclei with static deformations [2–9], for nuclei where vibrational degrees of freedom dominate [2,10], in systems where the effects of transfer channels [2,10,11] and multi-phonon excitations [12,13] are important, and where the influence of the projectile excitation is prominent [7,8,13].

The precise fusion data have stimulated advances in the quantitative application of the coupled-channels (CC) description of fusion, and many experimental barrier distributions have been well reproduced with various degrees of refinement of this model. The CC description is expected to be simpler for systems involving the fusion of closed-shell nuclei due to the presence of relatively few low-lying collective states. An example is the $^{16}\text{O}+^{144}\text{Sm}$ system, where a good description [10] of the experimental barrier distribution was obtained

with a simplified CC model [14,15]. This description was somewhat fortuitous in view of the approximations used in this model. An improvement in the description of the barrier distribution was achieved with more exact CC calculations [16–18] which correctly treated the excitation energies and the phonon character of the coupled states.

Given the current level of knowledge of the theoretical description of heavy-ion fusion, and the success of calculations in reproducing the shape of the measured barrier distribution for ^{16}O on ^{144}Sm , it might be expected that present models should be able to describe the fusion of ^{16}O with the doubly-magic nucleus ^{208}Pb . The $^{16}\text{O} + ^{208}\text{Pb}$ system is also one of the few cases where there is existing knowledge of important particle transfer channels. The fusion barrier distribution for the $^{16}\text{O} + ^{208}\text{Pb}$ reaction has been measured previously [19], however it was not possible to obtain an adequate theoretical description of its shape. This could have been due to shortcomings in the experiment or the simplified CC analysis used in calculating the theoretical barrier distribution. Improvements in the available techniques of precise fission cross-section measurements, including the use of fragment-fragment coincidences, were reason to re-measure the fusion excitation function for the $^{16}\text{O} + ^{208}\text{Pb}$ reaction.

The purpose of the current work was to find the cause of the previous disagreement between theory and data by comparing the newly measured barrier distribution with more exact CC calculations, and to identify the dominant couplings in the fusion of $^{16}\text{O} + ^{208}\text{Pb}$. The coupled-channels analysis of the new fusion data has proved to be more difficult than expected, and a complete description of the data has not yet been obtained.

II. EXPERIMENTAL RESULTS

The re-measurement of the fission excitation function for $^{16}\text{O} + ^{208}\text{Pb}$ was performed at the Australian National University using ^{16}O beams from the 14UD Pelletron accelerator. The beams were pulsed with bursts of 1 ns FWHM, separated by 106.6 ns. Beam energies used were in the range 75–118 MeV, in increments of 0.6 MeV up to 88 MeV. The absolute beam energy was defined to better than 0.05 MeV and the relative beam energy to better

than a few keV [2]. The target was 40–45 μgcm^{-2} of ^{208}PbO deposited on a backing of $\approx 10 \mu\text{gcm}^{-2}$ of C. The isotopic purity of the ^{208}Pb was $99.0 \pm 0.1\%$. Fission fragments were detected in two of the large-area multiwire proportional counters (MWPCs) of the CUBE detector system. One was positioned in the backward hemisphere covering the scattering angles $-171^\circ \leq \theta_{\text{lab}} \leq -94^\circ$, and the other in the forward hemisphere with $4^\circ \leq \theta_{\text{lab}} \leq 81^\circ$. The fission fragments were identified in an individual detector by their energy loss signal, and the time-of-flight measured relative to the pulsed beam.

In the measurement described in Ref. [19], only a single MWPC located in the backward hemisphere was used. However, in the present measurement, the front MWPC was operated in coincidence with the back fission detector, and the fission fragments were identified with the time-of-flight in one detector versus the time-of-flight in the other. This allowed good separation between the fission events from the $^{16}\text{O} + ^{208}\text{Pb}$ reaction and other reactions with the target, which were a problem for the low cross-sections in the earlier measurement. The fission cross-section was measured down to energies where the evaporation residue cross-sections were previously determined [19]. Two silicon surface-barrier detectors, located at $\pm 22.5^\circ$ to the beam axis, were used to monitor the Rutherford scattering for normalisation of the fission fragment yield. The fission fragment yields in the MWPCs were converted into fission cross-sections as described in Refs. [19,13].

The new fission excitation function is shown in Fig. 1(a), together with the results from the previous measurement [19], as indicated by the open circles in Fig. 1(a). The fusion cross-sections σ for $^{16}\text{O} + ^{208}\text{Pb}$ were obtained by summing σ_{fis} and the evaporation residue cross-sections published in Ref. [19], interpolating where necessary. The present data (solid circles) and previously published fusion cross-sections (open circles) are shown in Fig. 1(b). The fusion cross-sections from the new measurement are presented in Table I.

The fusion barrier distribution was obtained by evaluating the point difference formula of Ref. [2] using an energy step of $\Delta E_{\text{c.m.}} = 1.67 \text{ MeV}$. The resulting barrier distribution is shown in Fig. 2 by the solid circles. For comparison, the barrier distribution (open points) in Ref. [19] is reproduced, where each symbol represents one of the three separate passes

through the fusion excitation function. In Ref. [19], the barrier distribution was calculated with $\Delta E_{c.m.} = 1.86$ MeV. The difference in the two step lengths does not have any significant effect on the calculated barrier distributions since they are already smoothed by ≈ 2 MeV due to quantum tunnelling effects [1].

The new data are generally in good agreement with the previous measurement, but give a better defined barrier distribution. This is mainly due to the improved statistics, the clean identification of fission events made possible by operating two detectors in coincidence, and better definition and consistency of the angle between the beam axis and the fission detectors. The slight disagreement between the two barrier distributions can be largely attributed to three errant points in the original excitation function at $E_{c.m.} = 73.8, 74.3$ and 75.2 MeV, which differ from the current data by up to 5%. Since $d^2(E_{c.m.}^i \sigma)/dE_{c.m.}^2$ at an energy $E_{c.m.}^i$ is evaluated with a three-point difference formula, each wayward cross-section affects a total of three points, that point at $E_{c.m.}^i$, and its two neighbouring points at $(E_{c.m.}^i \pm 1.67)$ MeV. For example, the old cross-section at $E_{c.m.} = 75.2$ MeV was high with respect to the new measurement. This means that $d^2(E_{c.m.} \sigma)/dE_{c.m.}^2$ at $E_{c.m.} = 75.2$ MeV is lower than the new barrier distribution, and $d^2(E_{c.m.} \sigma)/dE_{c.m.}^2$ at both $E_{c.m.} = 73.3$ MeV and 77.1 MeV are high (see the encircled points in Fig. 2).

Nevertheless, the general features, such as the height of the main peak, and shape of the two barrier distributions are in good agreement.

III. COUPLED-CHANNELS ANALYSIS OF THE MEASURED FUSION BARRIER DISTRIBUTION

Several ingredients are required for a coupled-channels description of the fusion barrier distribution. Inputs to the model calculations include the nucleus-nucleus potential parameters, the coupling strengths of the vibrational states and their excitation energies. In addition, there are choices to be made regarding various assumptions and approximations used in the solution of the coupled equations.

A. The coupled-channels calculations

1. Nuclear potential parameters

The nuclear potential parameters were determined with consideration of two constraints: (i) fitting the high-energy fusion cross-sections, (ii) choosing a sufficiently deep nuclear potential, which is consistent with the ingoing-wave boundary condition used in the CC calculations. The measured fusion cross-sections at energies above the average barrier were fitted using a single-barrier penetration model, with an energy-independent nuclear potential, Woods-Saxon in form, with

$$V(r) = -V_0/(1 + \exp[(r - r_0A_P^{1/3} - r_0A_T^{1/3})/a]), \quad (1)$$

where V_0 is the depth, r_0 is the radius parameter, and a is the diffuseness of the nuclear potential. With V_0 chosen to be 50 MeV, r_0 and a were varied to obtain the best fit to σ . This resulted in the parameters $V_0 = 50$ MeV, $r_0 = 1.159$ fm and $a = 1.005$ fm, giving an average barrier $B_0 = 74.5$ MeV at a barrier radius of $R_B = 11.3$ fm with curvature for the average barrier of $\hbar\omega_0 = 3.07$ MeV. The excitation function and fusion barrier distribution associated with these single-barrier (SB) parameters are shown by the dot-dot-dashed lines in Fig. 3(a) and (b), respectively.

The above values for V_0 and r_0 could not be used in the CC codes because the potential depth was too shallow causing high- ℓ partial waves that should have been absorbed (contributing to the fusion cross-section) to be reflected at the barrier. To ensure that all the ingoing flux was absorbed inside the fusion barrier, a new set of potential parameters was obtained with the diffuseness parameter fixed at $a = 1.005$ fm, and V_0 was increased to 200 MeV, compensated by a reduction in r_0 to 0.978 fm to obtain the same fusion barrier $B_0 = 74.5$ MeV, which occurs at $R_B = 11.5$ fm with a curvature $\hbar\omega_0 = 3.87$ MeV. By making this adjustment in V_0 , the quality of the fit to the high-energy fusion cross-sections is reduced. However, this is not of concern for the following reasons.

The main aim of this analysis is the reproduction of the *shape* of the measured barrier distribution, a quantity which is insensitive to small changes in the potential parameters. In comparison, the high-energy fusion cross-sections are very sensitive to height of the average barrier, and can always be fitted by adjusting the potential parameters. However, since there exists some sensitivity of the calculated high-energy fusion cross-sections to the couplings [2], this would mean the nuclear potential parameters would need to be adjusted for each different coupling scheme if the fit to the high energy data is to be retained. Rather than re-fitting the high energy data after each new coupling scheme, the CC calculations were performed without any further adjustment to the bare nuclear potential. This meant that the calculated fusion cross-sections overestimated the data in the high energy region, see for example the CC calculations in Fig. 3(a). The data in the high energy region could be re-fitted with a slightly higher average fusion barrier, corresponding to a different set of potential parameters, but this would cause only a shift up in energy of the whole barrier distribution, without any appreciable change in its shape.

The diffuseness parameter obtained from the above procedure is significantly larger than that deduced from elastic scattering measurements [20], a result common to other fusion analyses [2]. The inconsistency between the diffuseness parameters obtained from fusion and elastic scattering data implies that the potential parameters obtained are specific to the data being fitted. It is also possible that the potential parameters obtained from a fit to the data in the high energy region are not applicable at energies in the barrier region, or below the lowest barrier. In this sense the potential parameters obtained are *effective* ones, and the true interaction potential remains an uncertainty in these calculations.

The effect of using a smaller diffuseness is shown in Fig. 3(a) and (b), where two calculations are compared, one with $a = 0.65$ fm and the other with $a = 1.005$ fm, both with the same average barrier $B_0 = 74.5$ MeV. Couplings to the single phonon states in ^{208}Pb are included in these CC calculations (see Sec. IIIB 1). For $E_{\text{c.m.}} < B_0$, the cross-section for the calculation with $a = 0.65$ fm falls less rapidly than the $a = 1.005$ fm case, since the smaller diffuseness gives a narrower barrier (larger $\hbar\omega_0$) and hence a larger barrier penetra-

bility. In the barrier region, a smaller diffuseness reduces the height of the main peak in $d^2(E_{\text{c.m.}}\sigma)/dE_{\text{c.m.}}^2$, due to the increase in the width of the tunnelling factor [1] which smooths the barrier distribution (see Sec. III C). These calculations demonstrate the effect on the calculated barrier distribution of the uncertainty in the appropriate choice of the diffuseness parameter. Further experiments are required to address this problem.

2. Approximations used in solving the coupled equations

In the coupled-channels calculations that follow, except for the FRESKO calculations, the no-Coriolis or isocentrifugal approximation [21–24] was used. This approximation has been shown [25,26] to be good for heavy-ion fusion reactions. The calculations included coupling to all orders in the deformation parameter for the nuclear coupling matrix. In the past, when making quantitative comparisons with the fusion data, the linear coupling approximation was often used. Here the nuclear coupling potential was expanded with respect to the deformation parameter keeping only the linear term. It was shown [16,25,27] that the agreement between the measured and calculated fusion cross-sections was improved with the inclusion of second-order terms. Later, Hagino *et al.* [16] demonstrated that, for heavy symmetric systems at least, the effect of inclusion of terms higher than second-order in the nuclear coupling potential was as significant as including the second-order term itself. Even though this effect was largest for heavy near-symmetric systems, it was also found to be significant for reactions involving lighter nuclei such as $^{16}\text{O}+^{144}\text{Sm}$.

The linear coupling approximation was retained for the Coulomb coupling potential since inclusion of terms of higher order has been shown to have only a very minor effect on the barrier distribution [16].

The excitation energies of the vibrational states were treated exactly in these calculations. Consequently, there were no approximations associated with the eigenchannel approach used in simplified CC analyses, such as those present in the code CCFUS [14].

B. Channel couplings

1. Coupling to single-phonon states in ^{208}Pb

Both ^{144}Sm and ^{208}Pb are spherical, vibrational nuclei with similar low-lying collective states, so it might be expected that the coupling scheme which was successful in the description of the barrier distribution for $^{16}\text{O} + ^{144}\text{Sm}$ would also provide a good description of the $^{16}\text{O} + ^{208}\text{Pb}$ reaction. The measured barrier distribution for the $^{16}\text{O} + ^{144}\text{Sm}$ reaction was well described by coupling to the single-phonon states in ^{144}Sm [10], where the dominant channel is the single-octupole phonon state. The analogous calculation for $^{16}\text{O} + ^{208}\text{Pb}$ is shown by the solid lines in Fig. 4(a) and (b). The calculation was performed with the CC code `CCFULL` [16,28], where fusion is simulated using the ingoing-wave boundary condition. Coupling to the 3_1^- and 5_1^- single-phonon states in ^{208}Pb was included, with the relevant parameters summarized in Table II. This calculation fails to reproduce the shape of the measured barrier distribution [see Fig. 4(b)]. Although the calculation produces a two-peaked structure, mainly due to coupling to the 3_1^- state in ^{208}Pb , there is still too much strength in the main peak of the theoretical barrier distribution, which implies that more coupling is required.

Additional coupling to other single-phonon states in ^{208}Pb produced no improvement in the agreement with the measured barrier distribution, due to the relative weakness of these couplings. In relation to the disagreement between theory and the data in Fig. 4(b), an initial impression is that the area of the calculated barrier distribution is larger than that of the measurement. This difference could be caused by a lower fusion yield resulting from a loss of flux due to incomplete fusion. Such an effect was recently observed [29] in the fusion of ^9Be on ^{208}Pb . However, evaluation of the area under $d^2(E_{\text{c.m.}}\sigma)/dE_{\text{c.m.}}^2$, a quantity which should be approximately proportional to the geometric area πR_B^2 , indicates that this is not the case. The area under the theoretical barrier distribution represented by the solid line in Fig. 4(b) is 4227 mb, implying a value of $R_B = 11.6$ fm for the average barrier

radius, obtained by simply equating the area with πR_B^2 . This compares with the area under the experimental barrier distribution of 3981 mb, implying a radius $R_B = 11.3$ fm. The difference between the theoretical and experimental areas is only 6%, 3.6% of which is due to use of the larger potential depth, $V_0 = 200$ MeV, which has a radius $R_B = 11.5$ fm instead of the best fit value of $R_B = 11.3$ fm for $V_0 = 50$ MeV. Thus, the mismatch between experiment and theory to the level of ≈ 2 -3%, is not due to incomplete fusion.

To obtain a successful theoretical description of the $^{16}\text{O}+^{208}\text{Pb}$ reaction, a coupling scheme that produces a barrier distribution with a shape corresponding to the measured one is required. Since the areas under the experimental and theoretical barrier distributions are in good agreement, the height of the main barrier in the distribution will be used as an indicator of the ability of theory to reproduce the overall shape of the experimental barrier distribution.

2. The effects of coupling to particle transfers

Attempts have been made previously to ‘explain’ qualitatively deviations between theory and experiment as being due to neglect of transfer couplings. Such an approach has been taken because of the difficulty of treating the transfer process in a realistic way, and the lack of knowledge of transfer coupling strengths. However in $^{16}\text{O} + ^{208}\text{Pb}$, some of the important transfer coupling strengths have been measured. To ascertain the significance of the effects of transfer couplings on fusion, both the transfer and inelastic channels (with coupling to all orders) should be considered simultaneously in the CC calculation. The effects of particle transfers on the fusion cross-sections and spin distributions for $^{16}\text{O} + ^{208}\text{Pb}$ have been calculated by Thompson *et al.* [30] at 8 energies between $E_{\text{lab}} = 78$ and 102 MeV, using the coupled-channels code **FRESCO** [31]. Here, those calculations have been repeated, with a minor modification to the nuclear potential in the entrance-channel mass partition, with coupling to all orders in the nuclear potential, and with smaller energy steps in order to obtain the barrier distribution. This was necessary since it was not possible to

treat transfer correctly using the code `CCFULL`. The details of this calculation are discussed below.

Before proceeding with the transfer calculations, the results of the two coupled-channels codes used in this work were compared. The comparison was made with a `FRESCO` calculation using parameters identical to the single-phonon calculation described in Sec. III B 1. The `FRESCO` calculation was performed with version `FRXX`, which includes a new option allowing coupling to all orders in the nuclear coupling potential, as in the calculation described in Sec. III B 1. The barrier distribution from `FRESCO` is shown by the dashed line in Fig. 4(b). There is very good agreement between it and the barrier distribution calculated using `CCFULL` [solid line in Fig. 4(b)]. The small difference between the solid and dashed lines in Fig. 4(b) may be due to the isocentrifugal approximation which was used in the `CCFULL` calculation.

Having established the agreement between the above two calculations for inelastic couplings, the effects of coupling to transfer channels were examined with `FRESCO`. In addition to the inelastic couplings, the following three transfer couplings were included, which are those included in the previous analysis [30]. The single-neutron pickup reaction ($^{16}\text{O},^{17}\text{O}$) with $Q = -3.2$ MeV, the single-proton stripping reaction ($^{16}\text{O},^{15}\text{N}$) with $Q = -8.3$ MeV and the α -stripping reaction ($^{16}\text{O},^{12}\text{C}$), where $Q = -20$ MeV, were included. The spectroscopic factors for the single-nucleon transfers were taken from Ref. [32], and in the case of the α -stripping couplings, were set to reproduce the measured transfer yield. Coupling to excited states in ^{17}O , ^{15}N , ^{207}Pb and ^{209}Bi was included as described in Ref. [30]. The real and imaginary potential parameters for all three transfer partitions were $V_0 = 78.28$ MeV, $r_0 = 1.215$ fm, $a = 0.65$ fm and $V_i = 10$ MeV, $r_{0i} = 1.00$ fm, $a_i = 0.40$ fm, respectively.

The barrier distribution from the `FRESCO` calculation including transfer is shown by the dot-dot-dashed line in Fig. 4(b). Compared to the case with no transfer, the main peak of the barrier distribution is shifted down in energy and its height is reduced, whilst the second peak in the distribution is smoothed in energy. Of the three transfer couplings considered in this calculation, the neutron-pickup transfer has the largest effect on the barrier distribution, since it is the most strongly populated transfer. Using a set of potential parameters for

the $^{17}\text{O}+^{207}\text{Pb}$ mass partition different to those quoted above, with a real diffuseness of $a = 1.005$ fm, had only a small effect on the shape of the barrier distribution. The 0.5 MeV shift downwards in energy of the barrier distribution is not problematic, since there is freedom to renormalise the bare potential to a value which will shift the theoretical barrier distribution back to its original position. Of importance here is the ability to reproduce the shape of the barrier distribution, and although the coupling to the transfer channels reduces the height of the main peak in the barrier distribution, it is not sufficient, implying that further couplings are required.

Additional transfer channels, which have been neglected in the present calculation, are unlikely to significantly improve the agreement, since the above three transfer couplings represent the most strongly populated transfers. The effects of additional transfers on the fusion cross-section were investigated in Ref. [33], where it was found that the α - and triton-pickup transfers had no effect on σ . The 2-neutron pickup, with $Q = -1.9$ MeV, did affect the fusion cross-section, although the increase in σ was at most a factor of 1.11 above the calculation without this transfer, at $E_{\text{lab}} = 78$ MeV. This compares with an enhancement in σ at the same energy of ≈ 2.5 between the transfer calculation with neutron-pickup, proton and α -stripping over the calculation without these transfer couplings.

3. The effects of coupling to the 3_1^- in ^{16}O

The treatment of projectile excitations in CC analyses deserves some comment. The measured barrier distributions for the reaction ^{16}O with various isotopes of samarium [2] showed no specific features associated with excitation of the octupole state in ^{16}O . It was shown in Ref. [2] that coupling to the 3_1^- state in ^{16}O at 6.13 MeV using the simplified CC code CCMOD [15], which uses the linear coupling approximation, resulted in a deterioration in the agreement with the measured barrier distribution. This effect is related to the neglect of the higher-order terms in the CC calculations [17,25]. Since the transition strength of the 3_1^- state in ^{16}O is large, higher-order terms should be included in the expression for

the nuclear coupling potential. When the 3_1^- state in ^{16}O was included with coupling to all orders in the nuclear potential, the theoretical barrier distribution was essentially restored to its shape before the inclusion of the projectile coupling [17]. However, the whole barrier distribution was shifted down in energy by a few MeV. This shift has been explained [34–36] in terms of the adiabaticity of the projectile excitation. When the excitation energy of a state is large, then the timescale of the intrinsic motion is short compared to the tunnelling time, allowing the projectile to respond to the nuclear force in such a way as to always be in the lowest energy configuration. This means that coupling to states like the 3_1^- state in ^{16}O , only leads to a shift in the average fusion barrier, and so is equivalent to a renormalisation of the effective potential.

In order to confirm the above result for the $^{16}\text{O}+^{208}\text{Pb}$ reaction, calculations were performed with coupling to the 3_1^- state in ^{16}O at 6.13 MeV using the code `CCFULL`. No better agreement with the shape of the measured barrier distribution resulted, causing only a shift in energy of the whole barrier distribution, without an appreciable change in its overall shape. An example of this effect is shown in Fig. 7(b).

In summary, the calculations described above, with a single-phonon plus transfer coupling scheme, were unable to describe the measured barrier distribution. In the next Section, the effects of a larger coupling space are explored. The following calculations result mostly from the code `CCFULL`. Due to the long computational time involved, `FRESCO` was used only to estimate the additional effects of coupling to transfer channels.

4. Coupling to the 2-phonon states in ^{208}Pb

In the doubly magic nucleus ^{208}Pb , the energy of the first 3^- state is at 2.614 MeV and is interpreted [37] as a collective octupole state because of its large $B(E3)$ value. In the harmonic vibrational model, the 2-phonon state would be expected [38] at an energy twice that of the single-phonon excitation. Hence in ^{208}Pb , the 2-phonon state $[3_1^- \otimes 3_1^-]$, consisting of the 0^+ , 2^+ , 4^+ , and 6^+ quadruplet of states, is expected [37] at the unperturbed energy of

5.228 MeV. There have been a number of searches for members of the 2-phonon quadruplet, including a recent $(n, n'\gamma)$ measurement [39] which found evidence for the existence of the 0^+ state at 5.241 MeV. A more recent measurement [40] using Coulomb excitation, did not identify any new state around 5.2 MeV, but was able to extract the $B(E3, 3_1^- \rightarrow 6_1^+)$ value for the lowest known 6^+ state at 4.424 MeV, whose strength suggested a strong fragmentation of the 2-phonon state in ^{208}Pb .

Because of the expected strong collective nature of the low-lying octupole state in ^{208}Pb , it is likely that 2-phonon excitations play some role in the fusion of ^{16}O on ^{208}Pb . The effects of the inclusion of 2-phonon excitations on the fusion barrier distribution have been investigated theoretically by Kruppa *et al.* [23] as well as Hagino *et al.* [41]. Recent experimental evidence has come from a measurement of the barrier distribution for the $^{58}\text{Ni}+^{60}\text{Ni}$ reaction [12], where it was demonstrated that fusion is sensitive to such complex multi-phonon excitations.

The barrier distribution shown by the solid line in Fig. 5 is a CCFULL calculation which includes, in addition to the 3_1^- and 5_1^- single-phonon states in ^{208}Pb , coupling to the double-octupole phonon in the target. This calculation was performed in the harmonic limit, where the energy of the $[3_1^- \otimes 3_1^-]$ state was taken to be 5.23 MeV, with the strength of coupling between the single- and 2-phonon states given by $\sqrt{2}\beta_3$, the coupling expected in the harmonic limit. The 2-phonon result produces a shoulder in the barrier distribution at $E_{\text{c.m.}} \approx 76$ MeV whilst reducing the height of the main barrier, leading to a minor improvement over the single-phonon coupling scheme. The inclusion of multiple excitations in the target, for example the $[5_1^- \otimes [3_1^- \otimes 3_1^-]]$ state, did not result in any significant difference to the barrier distribution given by solid line in Fig. 5, largely due to the fact that β_5 is very small. The additional inclusion of the 3_1^- state in the projectile, and mutual excitations of the projectile and target, was also found to have little effect on the shape of the calculated barrier distribution.

The next obvious choice to consider is coupling to the 2-phonon states in ^{208}Pb plus the transfer channels. Such a CC calculation was performed with FRESCO, and the results are

shown by the dashed line in Fig. 5. This causes a small shift in the barrier distribution to lower energies and an enhancement in the height of the shoulder at $E_{c.m.} \approx 76$ MeV over the single-phonon plus transfer calculation. Although the effect of these couplings are helpful, the resultant barrier distribution is still well short of a complete description of the data. One effect still not accounted for is multi-step transfer couplings. With the present CC codes, it was not possible to include transfer *from* the excited states in ^{208}Pb , and the effect of neglecting these channels on the barrier distribution is not known. However, it was possible to check if the anharmonicity of the 2-phonon states was responsible for the remaining disagreement. Below, the size of these effects are estimated.

5. The anharmonicity of the 2-phonon quadruplet in ^{208}Pb

When 2-phonon states were included in the coupling scheme for $^{16}\text{O}+^{144}\text{Sm}$, using the harmonic vibrational model, the good agreement between the measured and calculated barrier distribution was lost [42]. At first, this result was puzzling in that there is both theoretical and experimental evidence for the presence of double-octupole phonon states in ^{144}Sm [43]. However, deviations from the pure harmonic vibration model are expected to occur and the assumption of vibrational harmonicity for the coupling in ^{144}Sm is not correct. Subsequently it was demonstrated [18] within the framework of the interacting boson model, that when the anharmonicities of the double-phonon states were accounted for, the theoretical barrier distribution was restored to a shape matching the experiment. In fact, anharmonic coupling to the additional 2-phonon states marginally improved the agreement relative to the single-phonon description of the data.

It has been known for a long time that the 3_1^- state in ^{208}Pb has a large quadrupole moment, which is indicative of the anharmonic effects in octupole vibrations [37]. The anharmonic effects give rise to a splitting in energy of the 0^+ , 2^+ , 4^+ , and 6^+ members of the 2-phonon quadruplet in ^{208}Pb . In the Coulomb excitation search for 2-phonon states in ^{208}Pb by Vetter *et al.* [40], the authors found that the lowest lying 6^+ state populated

had a transition strength only $\approx 20\%$ of the harmonic $B(E3)$ value, indicating a possible fragmentation of the octupole vibrational strength of the 2-phonon state. Such a result has been supported by recent theoretical work [44], where calculations showed a strong fragmentation of the 6^+ member of the quadruplet.

The effect of the anharmonicities of the 2-phonon states in ^{208}Pb on the barrier distribution was estimated with a CCFULL calculation which included a reorientation term (see Eqs. (4) and (5) in Ref. [45]), with the spectroscopic quadrupole moment for the 3_1^- state of $Q_{3_1^-} = -0.34$ eb [46]. The results are shown in Fig. 6(a) for the case where the strength for the 2-phonon transition was $\sqrt{2}\beta_3$ (solid line) and when this strength was reduced by a factor 0.85 [dot-dot-dashed line in Fig. 6(a)]. The reduction factor applied to the pure harmonic octupole coupling strength was obtained from the results of Ref. [40]. The barrier distribution from the anharmonic calculation is a slight improvement over the harmonic result [dashed line in Fig. 6(a)] in region of 76 MeV. Any further increase in the degree of anharmonicity of the 2-phonon states (by reducing the energy of the 2-phonon state, for example) leads to a barrier distribution closer in shape to the single-phonon result. This effect is shown in Fig. 6(b), where an anharmonic calculation (solid line), with the energy of the 2-phonon at 4.424 MeV and the corresponding reduction in the coupling strength of 0.28 times that of the harmonic strength, is compared with the harmonic calculation (dashed line) and the single-phonon calculation (dot-dot-dashed line). The reduction factor of 0.28 was obtained in Ref. [40] from experimental observed intensity limits, which were then used to set limits relative to the expected harmonic E3 strength as a function of the energy of various 6^+ states in ^{208}Pb .

C. The effects of a smaller diffuseness parameter

As discussed earlier, the effects on the $^{16}\text{O}+^{208}\text{Pb}$ barrier distribution of using a smaller diffuseness for the nuclear potential lead to a reduction in the height of the main barrier (an increase in its FWHM). Such an effect can be explained with reference to Eq. (8) in Ref.

[1], since $d^2(E_{\text{c.m.}}\sigma)/dE_{\text{c.m.}}^2$ is proportional to $\pi R_B^2/\hbar\omega_0$ (the FWHM of the main barrier is proportional to $\hbar\omega_0$). In the $^{16}\text{O}+^{208}\text{Pb}$ reaction, a decrease in the diffuseness from $a = 1.005$ fm to $a = 0.65$ fm (resulting in an increase of $\hbar\omega_0$ from 3.85 MeV to 4.93 MeV) led to a reduction in the height of the main peak in the barrier distribution, as shown in Fig. 3(b). Even with this reduction to $a = 0.65$, close to the value of a obtained from fits to elastic scattering data [47], the height of the main peak in the experimental barrier distribution could not be successfully reproduced.

To obtain a reasonable reproduction of the measured barrier distribution, the diffuseness parameter had to be reduced to a value of $a \approx 0.40$ fm. However, this was done at the expense of the fit to the high-energy fusion cross-sections (see the discussion below). A CCFULL calculation with the potential parameters $V_0 = 283.6$ MeV, $r_0 = 1.172$ fm and $a = 0.40$ fm, chosen to give an average barrier of $B_0 = 77.6$ MeV, is shown in Fig. 7(b) by the dotted line. Here coupling to the 2-phonon states was included with the anharmonic values of 4.424 MeV for the energy of the 2-phonon states, and a reduction factor of 0.28 for the 2-phonon coupling strength, as discussed earlier. No transfer couplings were included in these calculations. After inclusion of the adiabatic 3_1^- state in ^{16}O , the barrier distribution shown by the solid line in Fig. 7(b) was obtained. The inclusion of the 3_1^- state in ^{16}O shifts the barrier distribution down in energy to provide a reasonable representation of the data. The third barrier distribution shown in Fig. 7(b) (dashed line) is a CC calculation with the $a = 0.40$ fm potential parameters, which give an average barrier of $B_0 = 77.6$ MeV, but *without* coupling to the 2-phonon excitations in ^{208}Pb . The difference between the 2-phonon (solid line) and single-phonon (dashed line) calculations for $a = 0.40$ fm is not as significant as the difference between the equivalent calculations with $a = 1.005$ fm, due to the additional smoothing of the barrier distributions that results from the smaller diffuseness (larger $\hbar\omega_0$).

Such a small value for the nuclear diffuseness is problematic in that the experimental fusion cross-sections could not be reproduced either at energies above or below the average barrier. A diffuseness of $a = 0.40$ fm, causes σ to fall less rapidly than the data in the low

energy region, as shown by the solid line in Fig. 7(a). And, in the high energy region, the calculation with $a = 0.40$ fm significantly overestimates the data, see the inset of Fig. 7(a). With any of the above coupling schemes, no single set of potential parameters was found that could simultaneously reproduce the shape of the experimental barrier distribution and the fusion cross-sections in the low and high energy region.

The results from the detailed CC analysis presented in this work are puzzling in view of the success obtained from other recent analyses of fusion barrier distributions [2,48]. In these results, the shapes of the theoretical barrier distributions matched well with the experimental ones after including the significant couplings expected to affect fusion. In contrast to this success, even after consideration of transfer and 2-phonon couplings in the $^{16}\text{O} + ^{208}\text{Pb}$ reaction, the theory was unable to reproduce the shape of the measured barrier distribution.

IV. SUMMARY AND CONCLUSION

In this work, fission cross-sections for the $^{16}\text{O} + ^{208}\text{Pb}$ reaction were re-measured with improved accuracy. The new data were found to be generally in good agreement with the earlier data, although some erroneous points in the original fission excitation function were identified. The barrier distribution resulting from the new data was found to be a smoothly falling function for energies above the average barrier.

In order to describe the shape of the measured barrier distribution, detailed CC calculations were performed, avoiding where possible less accurate approximations often used in simplified CC analyses, and exploiting existing knowledge of the particle transfers in the $^{16}\text{O} + ^{208}\text{Pb}$ system. It was found that coupling to the single-neutron pickup, single-proton and α -stripping transfers had a significant affect on the barrier distribution, although coupling to these transfers in addition to the 3_1^- and 5_1^- single-phonon states in ^{208}Pb , was not sufficient to explain the data. Transfer from excited states in ^{208}Pb were not included in the present calculations, and their effect on the shape of the barrier distribution is not known.

The effects of additional coupling to 2-phonon states in ^{208}Pb was explored, both in the harmonic limit and for cases that considered the anharmonicity of the 2-phonon states. Inclusion of the 2-phonon states in ^{208}Pb resulted in some improvement but still fell short of a complete description of the experimental barrier distribution.

A better reproduction of the experimental barrier distribution was obtained with a very large reduction in the nuclear diffuseness parameter, from a value of $a = 1.005$ to $a = 0.40$ fm. This approach to fitting the data was found to be unsatisfactory, since it destroyed the fits to the fusion cross-sections in the high and low energy regions. Also, a value of 0.40 fm for the nuclear diffuseness is significantly smaller than results obtained from analyses of elastic scattering data for the $^{16}\text{O} + ^{208}\text{Pb}$ system [30,49].

The results from fits to the high-energy fusion cross-sections for the $^{16}\text{O} + ^{208}\text{Pb}$ reaction, and other systems recently measured [2], also required a nuclear diffuseness larger than the value obtained from elastic scattering analyses. This result indicates that the procedure for determining the potential parameters used in this and the work of Ref. [2] may not be appropriate in the analysis of fusion. In elastic scattering, the more peripheral nature of the interaction means the system probes mainly the exponential tail of the nuclear potential. In contrast, fusion probes the potential at distances much closer to the fusion barrier radius. In this region, the Woods-Saxon parameterisation may not be an adequate representation of the true nuclear potential. Further work is required to determine the diffuseness of the nuclear potential appropriate to the analysis of precise fusion data.

Using the best available model for the description of heavy-ion fusion, it has been shown that the measured barrier distribution for $^{16}\text{O} + ^{208}\text{Pb}$ could not be reproduced with couplings to the lowest lying single- and 2-phonon states in ^{208}Pb and the major particle transfers. In view of the precision of the data, and the quality of the coupled-channels model used in its description, the disagreement between experiment and theory is very significant. Further work on the appropriate choice of the nuclear diffuseness, and a global analysis of all available reaction data, are required in order to improve the coupled-channels description of fusion for the $^{16}\text{O} + ^{208}\text{Pb}$ system.

ACKNOWLEDGEMENTS

K.H. and I.J.T. would like to thank the Australian National University for their warm hospitality and partial support where this work was carried out. M.D. acknowledges the support of a QEII Fellowship. K.H. acknowledges the support from the Japan Society for the Promotion of Science for Young Scientists.

REFERENCES

- [1] N. Rowley, G.R. Satchler, and P.H. Stelson, *Phys. Lett. B* **254**, 25 (1991).
- [2] J.R. Leigh, M. Dasgupta, D.J. Hinde, J.C. Mein, C.R. Morton, R.C. Lemmon, J.P. Lestone, J.O. Newton, H. Timmers, J.X. Wei, and N. Rowley, *Phys. Rev. C* **52**, 3151 (1995).
- [3] J.X. Wei, J.R. Leigh, D.J. Hinde, J.O. Newton, R.C. Lemmon, S. Elfström, and J.X. Chen, *Phys. Rev. Lett.* **67**, 3368 (1991).
- [4] R.C. Lemmon, J.R. Leigh, J.X. Wei, C.R. Morton, D.J. Hinde, J.O. Newton, J.C. Mein, M. Dasgupta, and N. Rowley, *Phys Lett. B* **316**, 32 (1993).
- [5] J.R. Leigh, N. Rowley, R.C. Lemmon, D.J. Hinde, J.O. Newton, J.X. Wei, J.C. Mein, C.R. Morton, S. Kuyucak, and A.T. Kruppa, *Phys. Rev. C* **47**, R437 (1993).
- [6] D.J. Hinde, M. Dasgupta, J.R. Leigh, J.P. Lestone, J.C. Mein, C.R. Morton, J.O. Newton, and H. Timmers, *Phys. Rev. Lett.* **74**, 1295 (1995).
- [7] J.D. Bierman, P. Chan, J.F. Liang, M.P. Kelly, A.A. Sonzogni, and R. Vandenbosch, *Phys. Rev. Lett.* **76**, 1587 (1996).
- [8] J.D. Bierman, P. Chan, J.F. Liang, M.P. Kelly, A.A. Sonzogni, and R. Vandenbosch, *Phys. Rev. C* **54**, 3068 (1996).
- [9] J.C. Mein, D.J. Hinde, M. Dasgupta, J.R. Leigh, J.O. Newton, and H. Timmers, *Phys. Rev. C* **525** R995 (1997).
- [10] C.R. Morton, M. Dasgupta, D.J. Hinde, J.R. Leigh, R.C. Lemmon, J.P. Lestone, J.C. Mein, J.O. Newton, H. Timmers, N. Rowley, and A.T. Kruppa, *Phys. Rev. Lett.* **72**, 4074 (1994).
- [11] H. Timmers, L. Corradi, A.M. Stefanini, D. Ackermann, J.H. He, S. Beghini, G. Montagnoli, F. Scarlassara, G.F. Segato, and N. Rowley, *Phys. Lett. B* **399**, 35 (1997).

- [12] A.M. Stefanini, D. Ackermann, L. Corradi, D.R. Napoli, C. Petrache, P. Spolaore, P. Bednarczyk, H.Q. Zhang, S. Beghini, G. Montagnoli, L. Mueller, F. Scarlassara, G.F. Segato, F. Soramel, and N. Rowley, Phys. Rev. Lett. **74**, 864 (1995).
- [13] D.J. Hinde, C.R. Morton, M. Dasgupta, J.R. Leigh, J.C. Mein, and H. Timmers, Nucl. Phys. **A592**, 271 (1995).
- [14] C.H. Dasso and S. Landowne, Comp. Phys. Comm. **46**, 187 (1987); J. Fernández-Niello, C.H. Dasso, and S. Landowne, *ibid.* **54**, 409 (1989).
- [15] M. Dasgupta, A. Navin, Y.K. Agarwal, C.V.K. Baba, H.C. Jain, M.L. Jhingan, and A. Roy, Nucl. Phys. **A539**, 351 (1992).
- [16] K. Hagino, N. Takigawa, M. Dasgupta, D.J. Hinde, and J.R. Leigh, Phys. Rev. C **55**, 276 (1997).
- [17] K. Hagino, N. Takigawa, M. Dasgupta, D.J. Hinde, and J.R. Leigh, Phys. Rev. Lett. **79**, 2014 (1997).
- [18] K. Hagino, N. Takigawa, and S. Kuyucak, Phys. Rev. Lett. **79**, 2943 (1997).
- [19] C.R. Morton, D.J. Hinde, J.R. Leigh, J.P. Lestone, M. Dasgupta, J.C. Mein, J.O. Newton, and H. Timmers, Phys. Rev. C **52**, 243 (1995).
- [20] P.R. Christensen and A. Winther, Phys Lett. B **65**, 19 (1976).
- [21] R. Lindsay and N. Rowley, J. Phys. G **10**, 805 (1984).
- [22] O. Tanimura, J. Makowka, and U. Mosel, Phys Lett. B **163**, 317 (1985).
- [23] A.T. Kruppa, P. Romain, M.A. Nagarajan, and N. Rowley, Nucl. Phys. **A560**, 845 (1993).
- [24] K. Hagino, N. Takigawa, A.B. Balantekin, and J.R. Bennett, Phys. Rev. C **52**, 286 (1995), and references therein.

- [25] H. Esbensen and B.B. Back, Phys. Rev. C. **54**, 3109 (1996).
- [26] O. Tanimura, Phys. Rev. C **35**, 1600 (1987); O. Tanimura, Z. Phys. A **327**, 413 (1987).
- [27] H. Esbensen and S. Landowne, Phys. Rev. C. **35**, 2090 (1987).
- [28] K. Hagino, N. Rowley, and A.T. Kruppa, Comp. Phys. Comm., in press.
- [29] M. Dasgupta, D.J. Hinde, R. D. Butt, R. M. Anjos, A.C. Berriman, N. Carlin, P.R.S. Gomes, C.R. Morton, J.O. Newton, A. Szanto di Toledo, and K. Hagino, Phys. Rev. Lett., **82**, 1395 (1999).
- [30] I.J. Thompson, M.A. Nagarajan, J.S. Lilley, and M.J. Smithson, Nucl. Phys. **A505**, 84 (1989).
- [31] I.J. Thompson, Comp. Phys. Reports **7**, 167 (1988).
- [32] M.E. Franey, J.S. Lilley, and W.R. Phillips, Nucl. Phys. **A324**, 193 (1979).
- [33] S.V.S. Sastry, Phys. Rev. C **58**, 3753 (1998).
- [34] H. Esbensen, J.-Q. Wu, and G.F. Bertsch, Nucl. Phys. **A411**, 275 (1983).
- [35] N. Takigawa, K. Hagino, M. Abe, and A.B. Balantekin, Phys. Rev. C. **49**, 2630 (1994).
- [36] K. Hagino, N. Takigawa, and A.B. Balantekin, Phys. Rev. C. **56**, 2104 (1997).
- [37] I. Hamamoto, Phys. Rep. C **10**, 63 (1974).
- [38] A. Bohr and B.R. Mottelson, *Nuclear Structure*, Vol. II (Benjamin, New York, 1975).
- [39] Minfang Yeh, P.E. Garret, C.A. McGrath, and S.W. Yates, Phys. Rev. Lett. **76**, 1208 (1996).
- [40] K. Vetter, A.O. Macchiavelli, D. Cline, H. Amor, S.J. Asztalos, B.C. Busse, R.M. Clark, M.A. Deleplanque, R.M. Diamond, P. Fallon, R. Gray, R.V.F. Janssens, R. Krücken, I.Y. Lee, R.W. MacLeod, E.F. Moore, G.J. Schmid, M.W. Simon, F.S. Stephens, and C.Y.

- Wu, Phys. Rev. C. **58**, R2631 (1998).
- [41] K. Hagino, S. Kuyucak, and N. Takigawa, Rev. C. **57**, 1349 (1998).
- [42] C.R. Morton, PhD thesis, Australian National University, (1995).
- [43] R.A. Gatenby, J.R. Vanhoy, E.M. Baum, E.L. Johnson, S.W. Yates, T. Belgya, B. Fazekas, Á. Veres, and G. Molnár, Phys. Rev. C **41**, R414 (1990).
- [44] V. Yu. Ponomarev and P. von Neumann-Cosel, Phys. Rev. Lett. **82**, 501 (1999).
- [45] E.M. Takagui, G.R. Satchler, H. Takai, K. Koide, and O. Dietzsch, Nucl. Phys. **A514**, 120 (1990).
- [46] R.H. Spear, W.J. Verneer, M.T. Esat, J.A. Kuehner, A.M. Baxter, and S. Hinds, Phys. Lett. B **128**, 29 (1983).
- [47] I.J. Thompson, M.A. Nagarajan, J.S. Lilley, and B.R. Fulton, Phys. Lett. B **157**, 250 (1985).
- [48] M. Dasgupta, D.J. Hinde, N. Rowley, and A.M. Stefanini, Annu. Rev. Nucl. Part. Sci., **48**, 401 (1998).
- [49] J.B. Ball, C.B. Fulmer, E.E. Gross, M.L. Halbert, D.C. Hensley, C.A. Ludemann, M.J. Saltmarsh, and G.R. Satchler, Nucl. Phys. **A252**, 208 (1975).
- [50] R.H. Spear, At. Data Nucl. Data Tables **42**, 55 (1989).
- [51] D.K. McDaniels, J. Lisantti, I. Bergqvist, L.W. Swenson, X.Y. Chen, D.J. Horen, F.E. Bertrand, E.E. Gross, C. Glover, R. Sayer, R.L. Burks, O. Häusser, and K. Hicks, Nucl. Phys. **A467**, 557 (1987).

TABLES

TABLE I. The fusion cross-sections for the $^{16}\text{O}+^{208}\text{Pb}$ reaction at the center-of-mass energy

$E_{\text{c.m.}}$		
E _{c.m.} (MeV)	σ (mb)	$\delta\sigma$ (mb)
69.97	0.24	0.01
70.53	0.70	0.004
71.09	1.83	0.01
71.64	4.28	0.02
72.20	8.27	0.04
72.76	14.5	0.07
73.31	23.4	0.1
73.87	35.4	0.2
74.43	50.0	0.3
74.99	67.0	0.3
75.54	87.0	0.4
76.10	107	0.5
76.66	129	0.7
77.21	152	0.8
77.77	175	0.9
78.33	197	1
78.88	223	1
79.44	245	1
80.00	270	1
80.56	295	2
81.11	318	2
81.67	343	2
82.78	385	2

85.01	487	3
87.24	568	3
89.73	662	3
91.70	715	4
96.15	847	4
100.72	949	5
105.06	1065	6
109.52	1133	6

TABLE II. The transition strengths $B(E\lambda)\uparrow$ and deformation parameters β_λ for $^{16}\text{O}+^{208}\text{Pb}$. The deformation parameters were calculated with a nuclear radius parameter of 1.06 fm. The parameters for the real nuclear potential are also given. In the CC calculations, the nuclear deformation parameters were set to be equal to the Coulomb deformation parameters.

Nucleus	λ^π	E^* (MeV)	$B(E\lambda)\uparrow$	β_λ	Ref.
^{208}Pb	3_1^-	2.615	$0.611 \text{ e}^2\text{b}^3$	0.161	[50]
	5_1^-	3.198	$\delta = 0.35^\dagger \text{ fm}$	0.056	[51]
^{16}O	3_1^-	6.129	$0.0015 \text{ e}^2\text{b}^3$	0.733^\ddagger	[50]
		V_0 (MeV)	r_0 (fm)	a (fm)	
		200.0	0.978	1.005	

[†] here δ is the deformation length. [‡] here a nuclear radius parameter of 1.2 fm was used.

FIGURES

FIG. 1. The (a) fission/ER and (b) fusion excitation functions for $^{16}\text{O} + ^{208}\text{Pb}$ from this re-measurement (solid circles) and the previous data of Ref. [19] (open circles). The ER cross-sections (open squares) are also from Ref. [19].

FIG. 2. The fusion barrier distribution from this measurement (solid circles) compared to the previous measurement [19] (open symbols). The uncertainties associated with the barrier distribution were obtained from the uncertainties in the fusion cross-sections, as described in Ref. [2]. See the text for an explanation of the encircled data points.

FIG. 3. The (a) fusion excitation functions and (b) barrier distributions for a single-barrier (SB) calculation (dot-dot-dashed line), and calculations using a single-phonon coupling scheme with two different sets of potential parameters [see Eq. (1)]: $V_0 = 200$ MeV, $r_0 = 0.978$ fm, $a = 1.005$ fm (solid line) and $V_0 = 277.5$ MeV, $r_0 = 1.10$ fm, $a = 0.65$ fm (dashed line). These calculations were performed with the CC code CCFULL.

FIG. 4. (a) The fusion excitation function calculated using CCFULL [28] with coupling to the 3_1^- and 5_1^- single-phonon states in ^{208}Pb (solid line). The dot-dot-dashed line is the same calculation but with the code FRESCO and with transfer included in addition to the single-phonon states. (b) The fusion barrier distribution calculated using CCFULL with coupling to the 3_1^- and 5_1^- single-phonon states in ^{208}Pb (solid line). The FRESCO result, performed with identical couplings (no transfer coupling), is given by the dashed line. When transfer, in addition to the single-phonon states in ^{208}Pb , is included this results in the barrier distribution represented by the dot-dot-dashed line.

FIG. 5. The barrier distribution for the single-phonon coupling scheme in ^{208}Pb (dotted line), with 2-phonon coupling (solid line), with single-phonon and transfer couplings (dot-dot-dashed line), and 2-phonon and transfer couplings (dashed line).

FIG. 6. (a) The effect on the barrier distribution when the anharmonicity of the 2-phonon states in ^{208}Pb are taken into account. The dashed line is the harmonic result where the energy of the 2-phonon state was taken as 5.23 MeV and the strength was $\sqrt{2}\beta_3$. The barrier distribution represented by the solid line includes the reorientation effect with a strength unchanged from the harmonic calculation. The dot-dot-dashed line is the same calculation as the solid line, but the strength has been reduced by a factor 0.85. Coupling to the transfer channels has not been included in these calculations. (b) The solid line is another anharmonic calculation, but assuming a lower energy for the 2-phonon states and with a significant reduction in the 2-phonon coupling strength (see text). This last result is compared with the same harmonic calculation shown in (a) [dashed line] and the single-phonon calculation (dot-dot-dashed line).

FIG. 7. (a) The fusion excitation function for a calculation with $a = 0.40$ fm and coupling to $(3_1^-, 5_1^-)$ single-phonon states in ^{208}Pb , anharmonic coupling to the 2-phonon states in ^{208}Pb (the strength of the 2-phonon coupling has been reduced by a factor 0.28 times the harmonic value, and the energy of the 2-phonon quadruplet is 4.424 MeV), and the 3_1^- state in ^{16}O . The dot-dot-dashed line is the single-barrier calculation with $a = 1.005$ fm. The inset compares these calculations with the data on a linear scale. (b) The solid line is the barrier distribution obtained from the fusion calculation represented by the solid line in (a). The dotted line is the equivalent calculation but without the coupling to the 3_1^- state in ^{16}O . The barrier distribution represented by the dashed line is equivalent to the calculation represented by the solid line but now only with coupling to the single-phonon states in the projectile and target. Coupling to the transfer channels has not been included in these calculations.

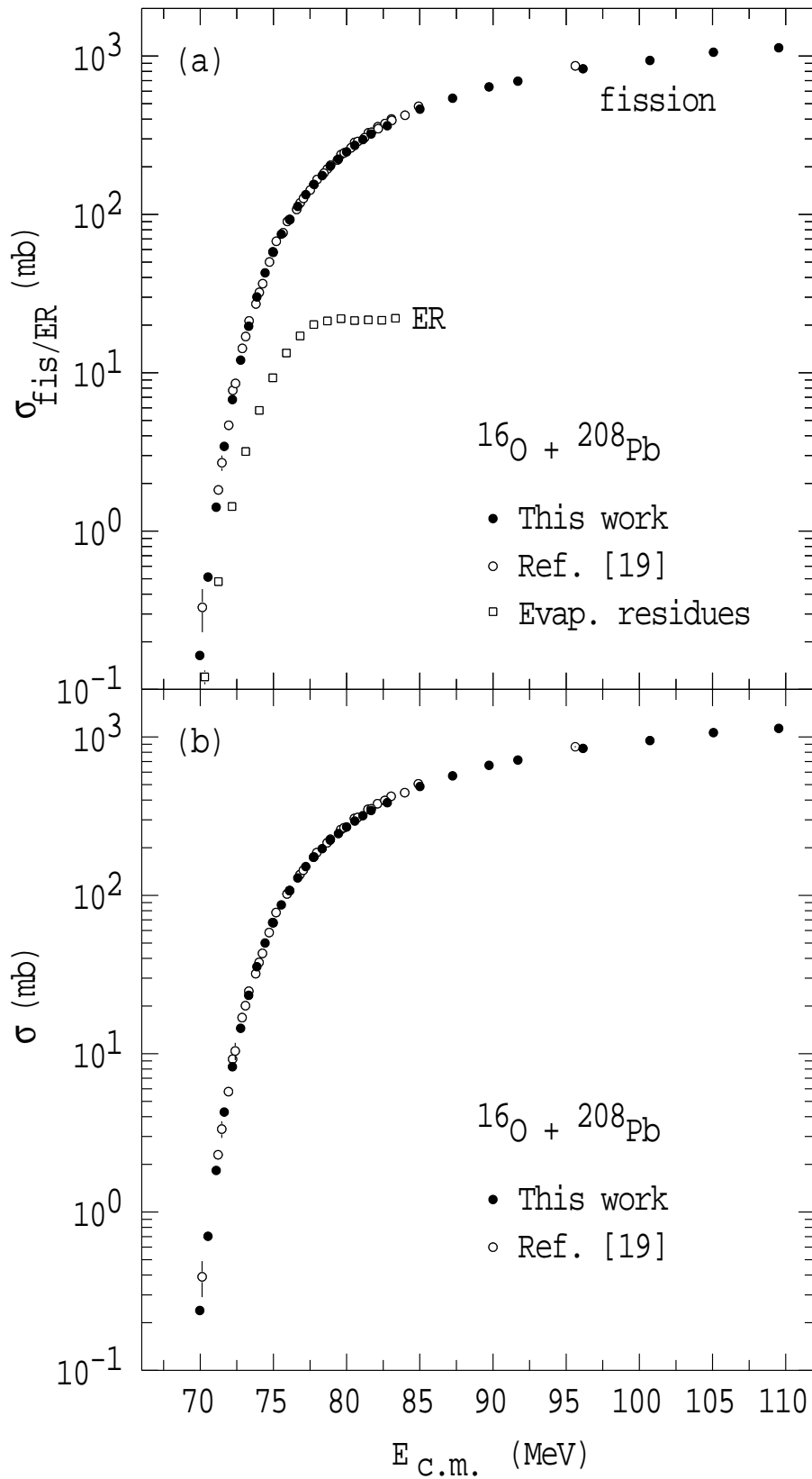


fig1 morton et al. 'Coupled-channels analysis of the...'

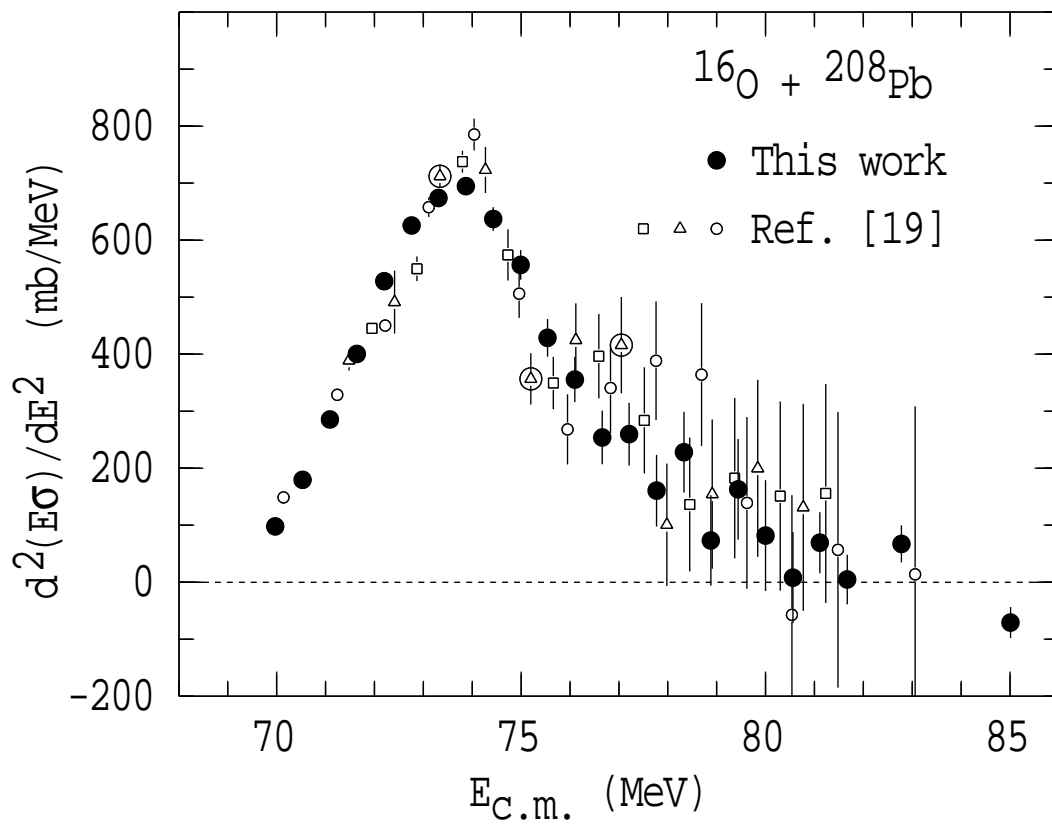


fig2 morton et al. 'Coupled-channels analysis of the...'

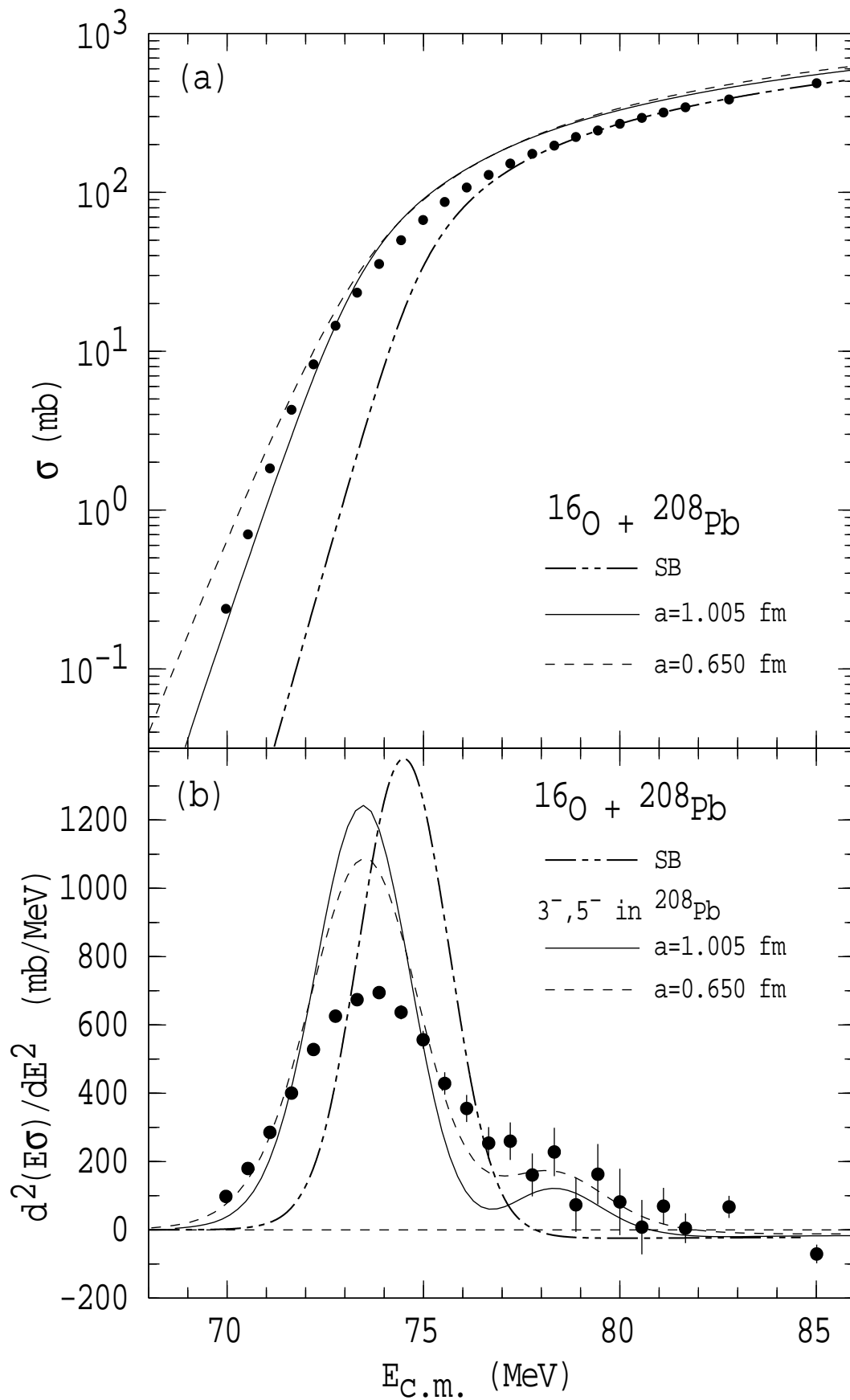


fig3 morton et al. 'Coupled-channels analysis of the...'

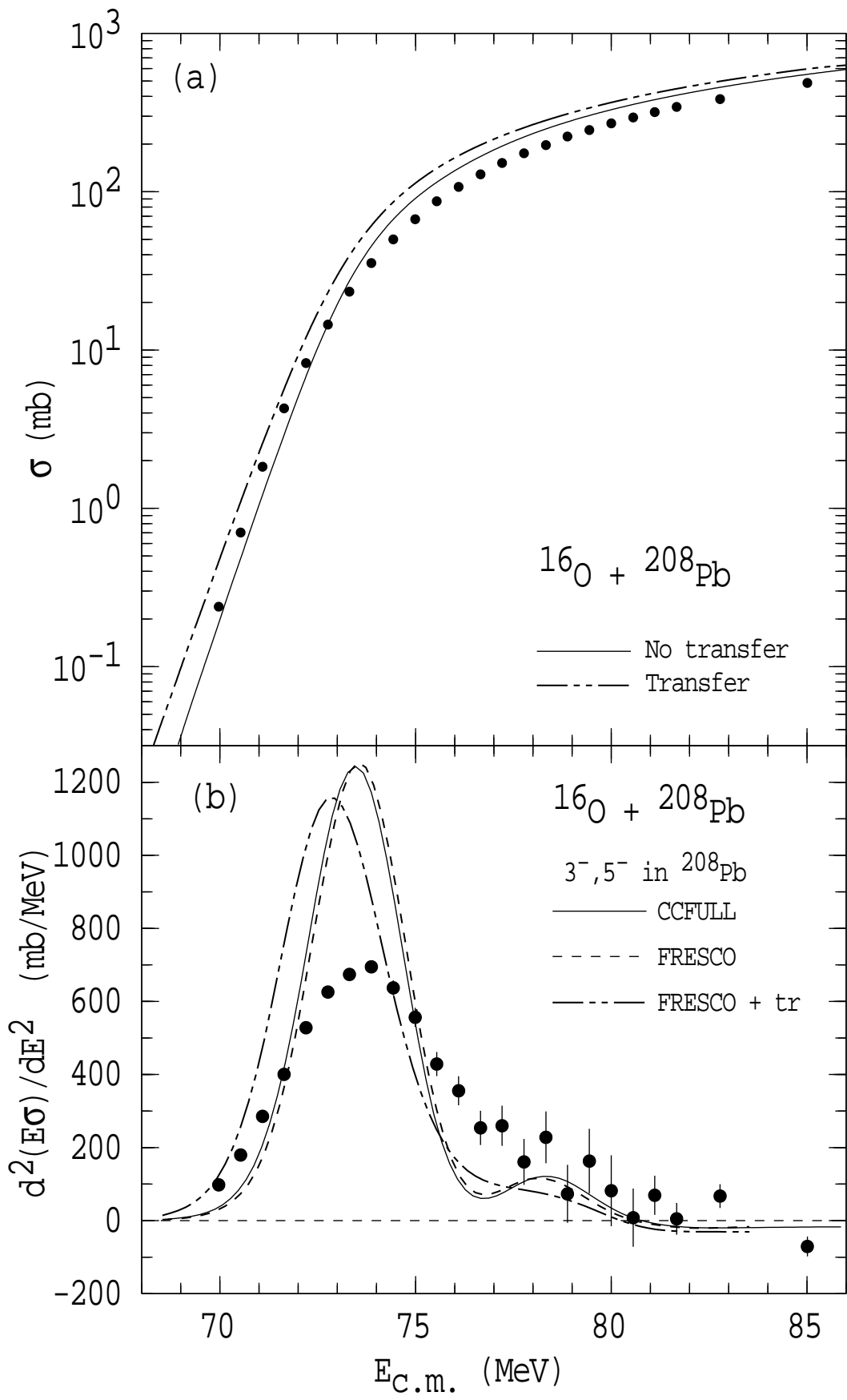


fig4 morton et al. 'Coupled-channels analysis of the...'

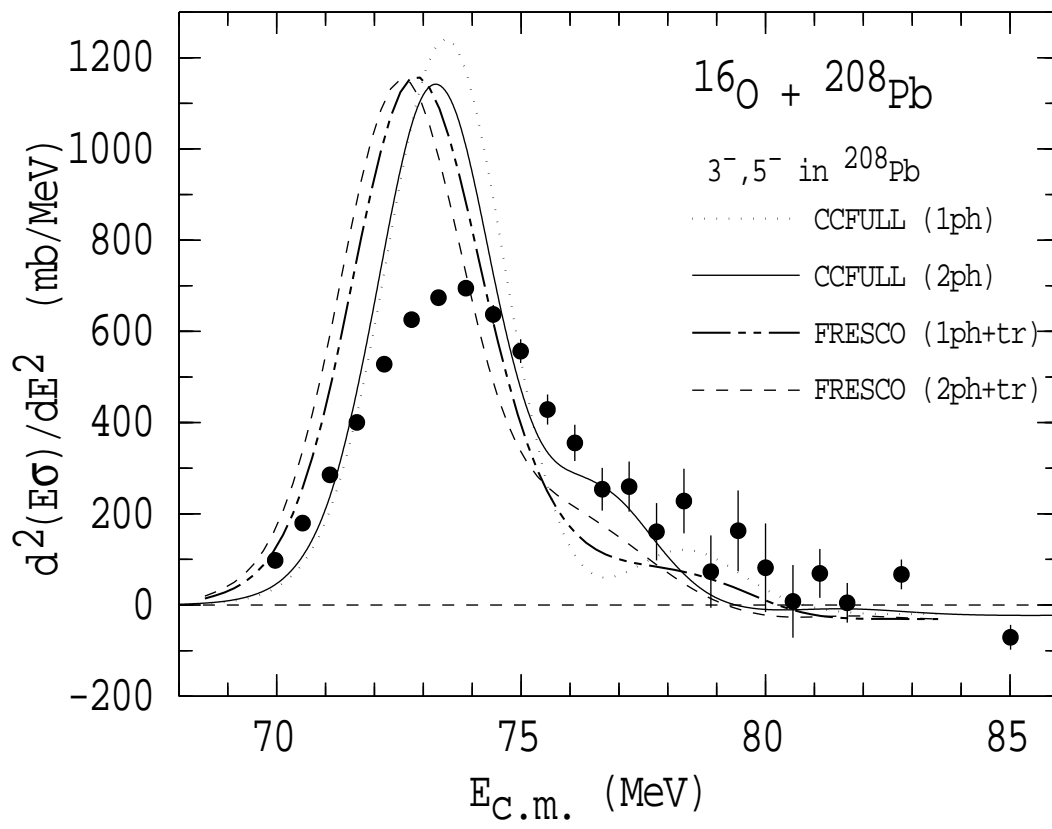


fig5 morton et al. 'Coupled-channels analysis of the...'

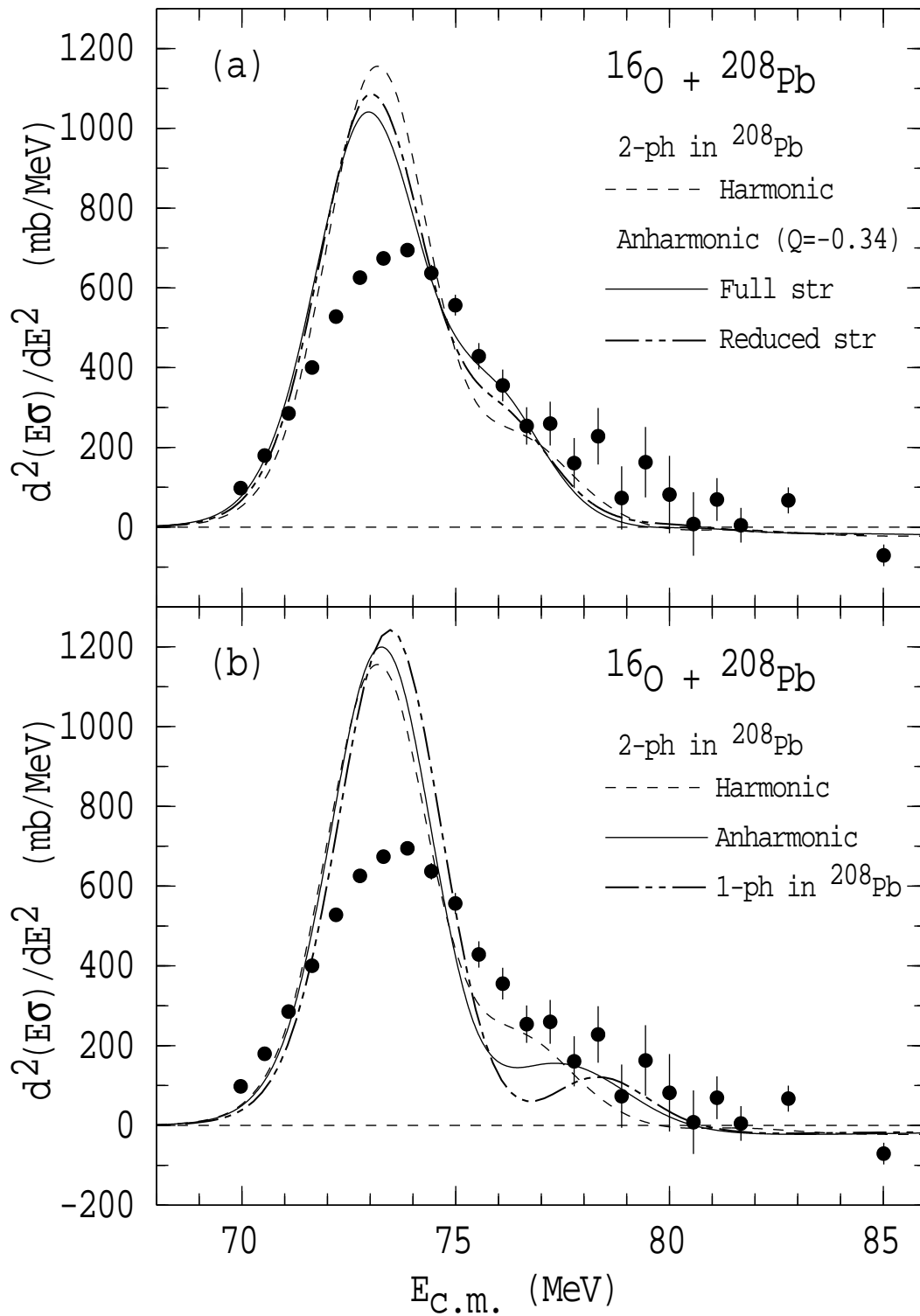


fig6 morton et al. 'Coupled-channels analysis of the...'

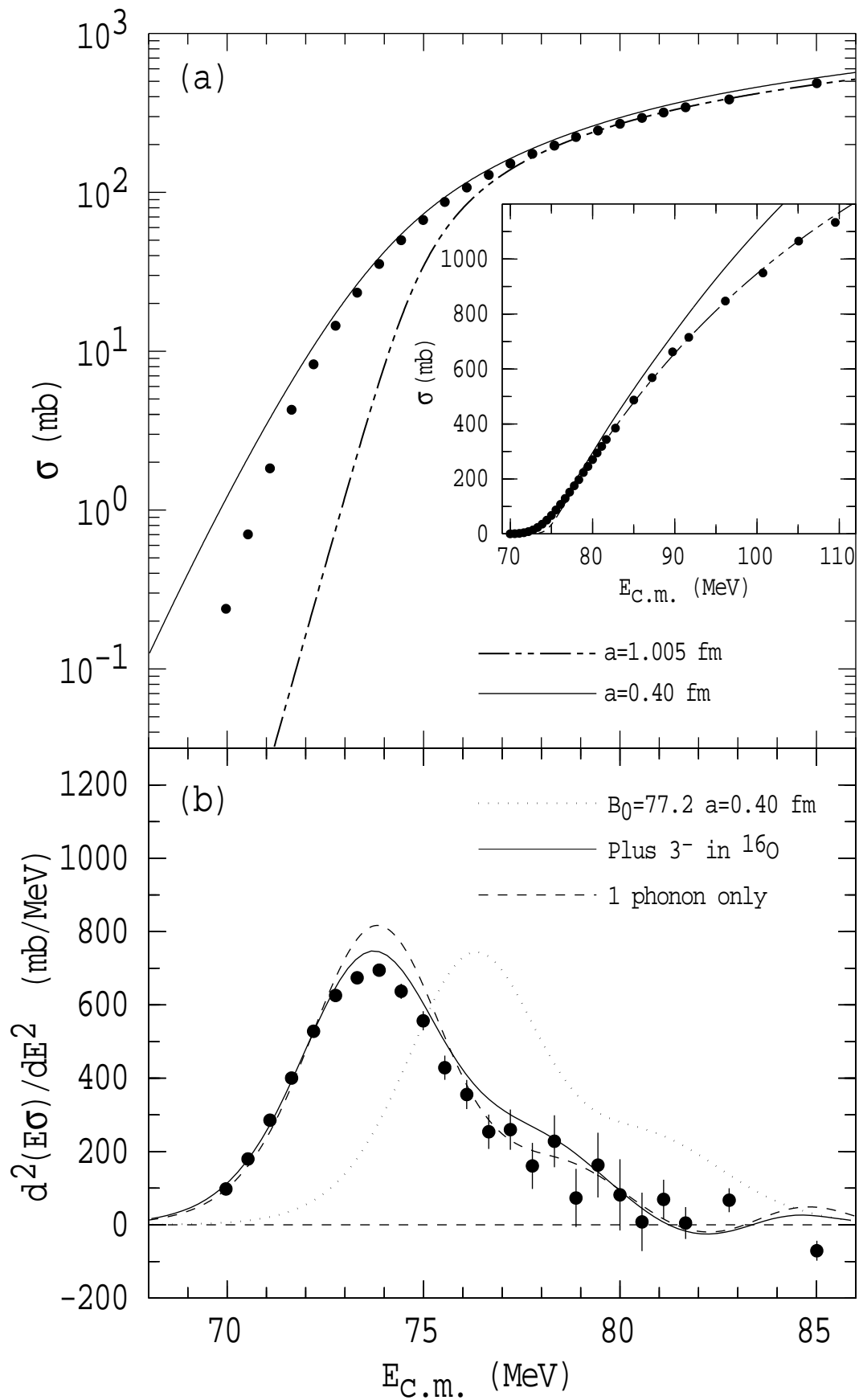


fig7 morton et al. 'Coupled-channels analysis of the...'